Cell-Scaffold Adhesion Dynamics Measured in First Seconds Predicts Cell Growth on Days Scale − Optical Tweezers Study

Rok Podlipec and Janez Štrancar*

Centre of Excellence NAMASTE, Jamova cesta 39, SI-1000 Ljubljana, Slovenia

Laboratory of Biophysics, Condensed Matter Physics Department, "Jožef Stefan" Institute, Jamova cesta 39, Ljubljana SI-1000, Slovenia

S *Supporting Information*

ABSTRACT: Understanding the cell−biomaterial interface from the very first contact is of crucial importance for their successful implementation and function in damaged tissues. However, the lack of bio- and mechano-analytical methods to investigate and probe the initial processes on the interface, especially in 3D, raises the need for applying new experimental techniques. In our study, optical tweezers combined with confocal fluorescence microscopy were optimized to investigate the initial cell−scaffold contact and to investigate its correlation with the material-dependent cell growth. By the optical tweezers-induced cell manipulation accompanied by force detection up to 100 pN and position detection by fluorescence microscopy, accurate adhesion dynamics and strength analysis was implemented, where several attachment sites were formed on the interface in the first few seconds. More importantly, we have shown that dynamics of cell adhesion on scaffold surfaces correlates with cell growth on the days scale, which indicates that the first seconds of the contact could markedly direct further cell response. Such a contact dynamics analysis on 3D scaffold surfaces, applied for the first time, can thus serve to predict scaffold biocompatibility.

KEYWORDS: *cell growth, cell adhesion, single cell manipulation, optical tweezers, scaffold biocompatibility*
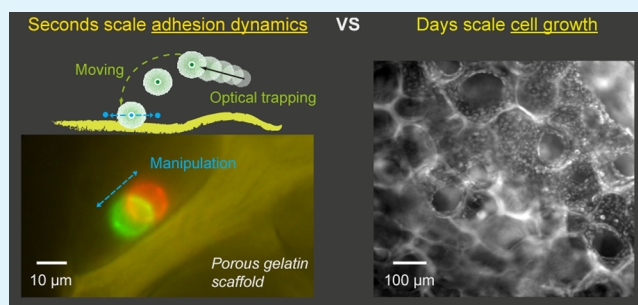
INTRODUCTION

In recent years, tissue engineering in regenerative medicine (TERM) has focused strongly on the investigations of material−cell interactions to understand biocompatibility of the materials.[1] An order-of-magnitude increase of research article publications in the past decade[2] with increasing interdisciplinarity and yet relatively small number of commercially available materials,[3] indicates that biomaterial−tissue interface science needs more conceptual breakthroughs to better understand biocompatibility.

Although cell adhesion is the very first process that reflects the specific properties of the material, the majority of the studies is focused on material−cell interaction by exploring the response of the cells with already established focal complexes between membrane integrins and specific ligands on biomaterial sites.[4] The studies of cell behavior comprise investigation of specific cell dynamics during and after establishing focal adhesions,[5,6] exploring the signaling processes governed by mechanotransduction,[7] or revealing specific gene expression and differentiation, proliferation, and migration through the biomaterial matrix, the so-called scaffold.[8] On the other hand, the intrinsic material−cell interaction that is expected to be reflected and exposed during the initial contact can be modulated by the cell-secreted components that can mask the real material properties making the choice of the experimental detection even more important.

Quick review through the literature reveals that material−cell interaction is commonly investigated by cell counting assays applied hours after most likely occurring adhesion.[9−11] To study the mechanics of the initial attachment, few methods with different force and time detection range have been implemented. Among them, spinning disk technique[12] and microfabricated post array detection[13] enable force measurement of cell adhesion up to hundreds of nanonewtons, while the micropipette aspiration technique[14] and centrifugation assay[15] allow this up to hundreds of piconewtons. However, in all the described methods the adhesion is studied minutes to hours after initial cell−material contact; thus, it is unable to identify the first molecular events responsible for further strong integrin-based adhesion. Furthermore, the above experimental setups lack a direct efficient probing of cell−substrate interface, which makes the interpretation of the behavior of cell on the interface even more difficult. To address this issue, two advanced methods, single-cell force spectroscopy (SCFS) using atomic force microscopy (AFM)[16] and optical tweezers (OT),[17] have been successfully implemented allowing accurate investigation of the adhesion dynamics of single cells in the first seconds to minutes after the initial contact with approximate

piconewton accuracy,[18,19] while, for the detection of single molecular events at the very beginning of the contact, new methods have recently been developed, a tension gauge tether (TGT) approach to measure single integrin-ligand bonds[20] and molecular tension-based fluorescence microscopy (MTFM), to measure piconewton forces exerted by cell surface receptors.[21] Due to the force resolution of less than piconewton[22,23] and particularly the ability of 3D manipulation of cells with independent 2D or 3D control,[24] accompanied by easier handling and visualization of the investigated systems such as presented in our study, OT is considered favorable over SCFS and the latter single molecular detection methods. However, the physical principles of OT[25] limit the force detection range to a maximum of a few hundred piconewtons which can balance only about a few hundred H bonds. OT is commonly combined with an imaging techniques such as fluorescence microscopy,[26−28] convenient to investigate complex cell–material[29] or cell–cell adhesions.[30,31]

In our work, the application of OT combined with fluorescence microscopy was optimized to study the initial cell–material contact and address the biophysical background of the material-dependent cell-adhesion. Biocompatibility of the 3D gelatin porous scaffolds that has been previously studied through polymer molecular mobility[32] has now been addressed in the perspective of the adhesion dynamics with the optical tweezers used for cell manipulation and force detection coupled to confocal fluorescence microscopy used for an accurate scaffold surface, cell, and OT position detection through a two-photon excitation.[33]

■ EXPERIMENTAL SECTION

Materials. Gelatin type B, sodium phosphate monobasic dihydrate, sodium phosphate dibasic heptahydrate, sodium carbonate, and sodium bicarbonate were purchased from Sigma-Aldrich as a scaffold material and its fabrication solution compounds. 1-Ethyl-3(3-(dimethylamino)propyl)-1-carbodiimide hydrochloride (EDC; Carbosynth) and N-hydroxysuccinimide (NHS; Sigma-Aldrich) were used as cross-linking agents for gelatin polymers. Fluorescein isothiocyanate isomer I (FITC; Invitrogen) was used as a fluorescent probe to label the side chains of gelatin polymers. L929 mouse fibroblasts were purchased from tissue engineering company Educell d.o.o. (Ljubljana, Slovenia), whereas fatty acid fluorescent probe SPP-158 (Figure S5 in the Supporting Information) was employed to stain cell membranes obtained as a generous gift from the Faculty of Pharmacy (University of Ljubljana, Slovenia). Si microspheres (Bangs Laboratories, Inc.) of the sizes 2.3, 5, and 7 μm were used for the optical tweezers force calibration and for cell–scaffold adhesion characterization.

Scaffold Preparation. Gelatin scaffolds were prepared using temperature controlled cryo-gelation[34] with tunable freezing and thawing cycle as described before.[32] Briefly, 10% (w/v) of gelatin in phosphate (pH 7.5) and bicarbonate buffer (pH 9.5) was heated up to a temperature of 50 °C to overcome the sol–gel or helix–coil transition to completely suppress nucleation of helical aggregates.[35] Thus, efficient covalent functionalization of amine groups was done with the fluorescent FITC isothiocyanate probe (reactive isothiocyanate group). Buffer solution of EDC and NHS in the molar ratio 4:1 (V = 0.7 mL) was mixed with the heated functionalized gelatin solution (V = 6 mL) to cross-link the polymer matrix simultaneously with cryogelation process. Different concentrations with respect to gelatin free amine groups were used (Table 1) to produce scaffolds with variable properties. Cryogelation was done in the Teflon Petri dishes (d = 50 mm) placed on the temperature-controlled plate. After final thawing, fabricated scaffolds were dialyzed against the appropriate buffer to remove all nonreacted cross-linkers and labeling probes. Scaffolds were sterilized with 70% ethanol solution for 2 h and UV light exposure in the sterile atmosphere for 30 min prior cell growth

Table 1. Preparation Parameters of Investigated Scaffolds

samples	buffer pH	n(EDC):n(free COOH sites)[a]
scaffold 1	9.5	0.15
scaffold 2	9.5	1
scaffold 3	7.5	0.15
scaffold 4	7.5	1

[a]Molar ratio.

and cell adhesion dynamics experiments. Finally, they were dialyzed three times with sterile PBS (V = 50 mL), changed each day, and stored at 5 °C. Before measurements, scaffolds were cut into thin slices (5 mm × 5 mm × 5 mm) and tempered in PBS at 37 °C for 10 min.

Scaffold Characterization. Morphological, mechanical, and molecular properties of scaffolds were investigated and are thoroughly presented in the Supporting Information, pages 2−6, Figures S1−S4. Briefly, morphological analysis was done using confocal fluorescence microscopy (CFM), where polymer primary amine groups were labeled with FITC-isothiocyanate during scaffold fabrication to enable detection. Mechanical analysis was done by atomic force microscopy (AFM), where a nanoindentation technique was used to measure the elastic modulus. Last, the molecular dynamics/mobility of polymer side chains in the scaffold structure was measured using electron paramagnetic spectroscopy (EPR). A methodology for morphological and molecular analysis was described in detail in our previous paper[32] and is briefly described in the Supporting Information.

Cell Preparation for Cell Growth Analysis. L929 fibroblasts were cultured in DMEM containing 10% fetal bovine serum (FBS) and 1% penicillin/streptomycin (PS) at 37 °C and 5% CO_2. Cells were harvested from the culture plate at the confluent state by incubating in trypsin solution for 2 min at 37 °C. Cells were resuspended with serum-supplemented DMEM and transferred into the 15 mL test tubes (V = 5 mL) with the cell concentration of 10^5 cells/mL. Sliced scaffolds of the size 5 mm × 5 mm × 5 mm were added into cell suspension and a gentle stirring method using a temperature controlled shaking bath (Julabo) was used for 2 min for the controlled cell administration onto the scaffolds. Seeded scaffolds were removed from cell suspension, put into 96-well plates, resuspended with serum-supplemented DMEM, and transferred into the cell culture incubator.

Cell Growth Analysis by CFM and by Viability Assay. Cell membranes were stained with SPP158 diluted in DMEM at the concentration of c = 5 × 10^{-7} M for 5 min. Prior the analysis, cell staining suspension was changed with body temperature serum-supplemented DMEM to remove all excess fluorescent probe. CFM images were taken under 15× magnification. Cell number was calculated via thresholding the cell intensity against the darker environment as described before.[32] Briefly, the density of cells was calculated as the number of cells per scaffold surface available for cell growth (N_{cells}/unit²), with the essential role of the morphology, which had to be thoroughly characterized.

To quantify cell growth with a complementary test, fluorometric analysis using Resazurin cell viability assay (Invitrogen) was applied. Fluorescence intensity was measured 4 h after Resazurin incubation at the concentration of c = 500 μM in DMEM in the corresponding emission filter of 580−650 nm. The reference signal of DMEM was measured to subtract the background. To estimate the total number of cells on scaffolds, Resazurin calibration curve were done by measuring the fluorescence signal at different concentrations of cells grown in cell culture plates (Figure S6 in the Supporting Information).

The viability assay was measured six times for each scaffold, whereas CFM was applied three times with five images analyzed for each sample. The analyses were done on the first and seventh day after cell scaffold culturing.

Cell Preparation for Adhesion Dynamics Analysis. Following the protocol of culturing and trypsinization described above, cells were suspended in serum-supplemented DMEM containing fluorescently labeled fatty-acid membrane probe SPP158 at concentration of c = 5 × 10^{-7} M for 1 min to stain the cell membranes for fluorescence detection. Cell suspension (4 × 10^5 cells/2 mL) was centrifuged at

300g for 2 min to remove the supernatant with nonlabeled probe and resuspended in serum-supplemented DMEM or PBS at a concentration of 10^5 cells/mL. A 400 μL portion of cell suspension was seeded on a tempered scaffold placed in a Nunc Lab-Tek chambered cover glass suitable for high magnification and highly efficient optical manipulation and detection.

Cell Adhesion Analysis by Optical Tweezers (OT) and CFM Detection. Cell manipulation with optical tweezers was performed immediately after transferring the cell suspension into the sample chamber containing the scaffold sample. Experiments were performed on the inverted microscope Nikon Eclipse TE 2000-E, implemented with optical tweezers system (Tweez 200si, Aresis) and CARV II unit (BD Biosciences) for the fluorescence detection.[36] Cells were trapped in the close proximity to the scaffold surface individually and then accurately positioned in direct contact with the scaffold surface (Scheme 1a). For cell manipulation in the 3D, acousto-optic deflection

Scheme 1. Scheme of Cell−Scaffold Adhesion Experimental Setup (a) Preparing the System for Cell Adhesion Experiments—Trapping, Bringing, and Manipulation of Cells on the Scaffold Surface; (b) Cell Adhesion Analysis with Two Different Scenarios: When Adhesion Strength Is Measured after a Particular Time of Contact (Static Conditions, No F_{ext} Induced on the Interface) or Measured in Time (Dynamic Conditions, F_{ext} Induced on the Interface by OT Manipulation in the Parallel Direction to the Scaffold Surface)[a]
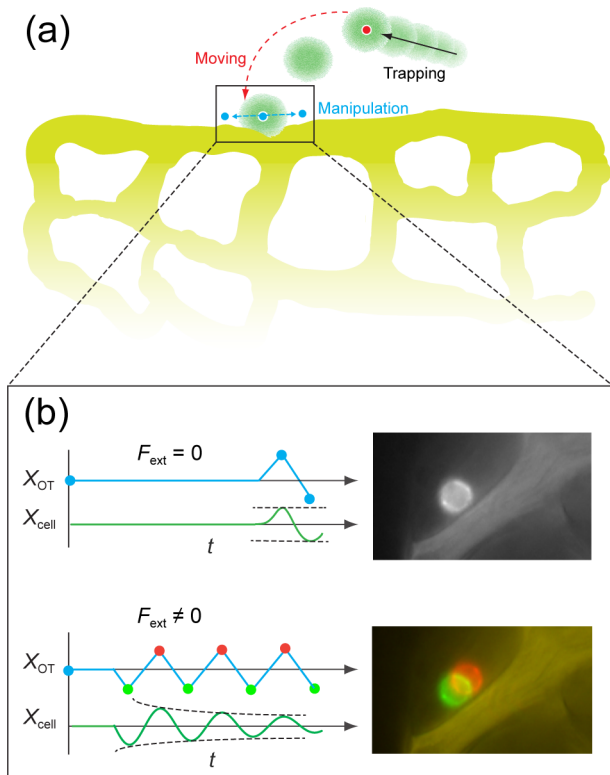
[a]Cell displacement amplitude (dashed black line) was tracked to evaluate the binding force.

system (AOD) mode of the optical tweezers system combined with the z-stage position controller was used. A high Z-axis working distance of 170 μm and high trapping power for sufficient 3D manipulation in the whole Z working distance was enabled by high numerical aperture (NA = 1.27) of the 60× water immersion objective (Nikon) and strong infrared (IR) laser source of 5 W. Due to localized cell heating[37] and known photothermal damaging effect on cells produced by strong focused optical fields,[17,38] the laser power applied

on cells was limited to P = 500 mW, with the maximum exposure time of 1 min. The limiting power was defined by measuring power dependent focal heating using temperature sensitive quantum yield of fluorescent NBD attached to the probe SPP268 (Figure S5 in the Supporting Information) and by modeling using heat equation, where both nicely correlated.[39] The temperature in the focal volume was increased for nearly 7 °C and for that reason the heater of the cell chamber was tuned on a 30 °C to not exceed 37 °C in the exposed volume. With such power, enough optical force was induced to counteract relevant forces at the interface during and after the adhesion governed by specific ECM proteins,[19,40] which is in the range from a few to tens of piconewton. More precisely, the setup enabled force measurement up to 100 pN without imposing high thermal stress onto the cells and maintaining biologically relevant conditions. Adhesion analyses were done approximately at the constant height of 50 μm to avoid trapping force being varied by the height.[41]

For a quantitative characterization of the forces on the scaffold−cell adhering interface, OT force calibration was required first. Generally, a trapping stiffness k_{trap} and a maximal trapping force F_{max} are measured by implementing different techniques of a trapped particle tracking such as monitoring the phase lag between the trap and the moved object when imposing a forced oscillation,[29,42] applying thermal fluctuation method for a trapped object,[42,43] or applying dynamic viscous drag force approach on a trapped object.[43,44] In our study, the latter method was used to calculate F_{max}, which was done through the measurement of a critical velocity of the surrounding fluid at which its drag force on the trapped object according to Stokes levels with the maximum opposite directed restoring gradient trapping force F_{grad}, which is exactly F_{max}. Characterization was done using trapped 2.3, 5, and 7 μm sized Si microspheres, placed in a fixed trap and moving motorized sample stage with a resolution of 40 nm. The indirect calibration with microspheres was applied due to nonhomogeneous cell surface and its prolate spheroidal shape in the OT field, which prevent accurate flow velocity determination.[45] Afterward, the calibrated force on microspheres was used to calibrate force on a cell, loosely bound to the scaffold surface, by comparing its displacement exerted directly by OT and indirectly by microspheres trapped in OT with predefined F_{max} = 100 ± 5 pN for the laser power P = 500 mW (see the movie clip am5b00235_si_002.avi in the Supporting Information). On the basis of the comparison of displacement amplitudes of an adherent cell, the maximal exerted force directly by OT was calculated F_{max} = 100 ± 10 pN. This force was induced when OT trap had been brought from the center of cell toward the cell membrane, where dense membrane structures accompanied by cytoskeleton form the highest difference in refractive index (with respect to water). The criteria for successful cell adhesion was defined as the event when OT induced F_{max} could not detach the cell bound with $F_{bind} > F_{max}$.

After trapping and bringing the cell to a direct contact with scaffold (Scheme 1a), two different cell adhesion analyses scenarios were implemented (Scheme 1b). In the first case, cell adhesion was analyzed after particular time of the contact during which no external force was exerted on the cell. Briefly, cell attachment was analyzed by monitoring the amplitude of cell displacement resulted from a single, two seconds lasted OT move (dashed line in Scheme 1b) with the amplitude of 30 μm parallel to the scaffold surface, conducted after the initial contact time of 1−20 s. The time window was chosen according to the highest OT force sensitivity as measured by preliminary experiments and latter adhesion strength according to the force induced cell displacement, described in more details in the Results and Discussion section. Experiments were done in DMEM growth media and in PBS with 50 to more than 100 tests to reach adequate statistics. Examples of cell−scaffold adhesion experiment are shown in the movie clips am5b00235_si_003.avi to am5b00235_si_006.avi in the Supporting Information.

In the second case, the time track of adhesion was analyzed by measuring change in the amplitude of cell displacement through periodical OT moves across the cell (dashed curve in Scheme 1b). Under such a scenario, an external force was constantly introduced on the cell, where its magnitude depended on the relative OT trap

position within the cell. Thus, its effect on the lifetime of bonds[46] as well as on their dissociation rate[47] needed to be considered. In our model, cell displacement was inversely related to the number of binding sites established between the cell and the scaffold surface assuming interactions are homogeneous and nonspecific.

Cell displacement was analyzed by acquiring cell positions through the cell shape fitting from CFM images with 100 nm resolution. High contrast of the cell shape was achieved through cell labeling with fluorescent membrane probe.

■ RESULTS AND DISCUSSION

Scaffold Biocompatibility. To check whether cell adhesion dynamics constitutes biocompatibility concept, reference fibroblast growth was monitored first on a set of the 3D gelatin porous scaffolds fabricated with different parameters of chemical cross-linking and pH (Table 1) resulting in different morphology (Figure 1) and other properties (see the Supporting Information). Scaffolds 1−4 (Figure 1a−d, respectively) were used to measure cell growth during the first day as well as the first week via CFM and cell membrane staining. Although some differences can be identified already after 1 day of culture, especially between a
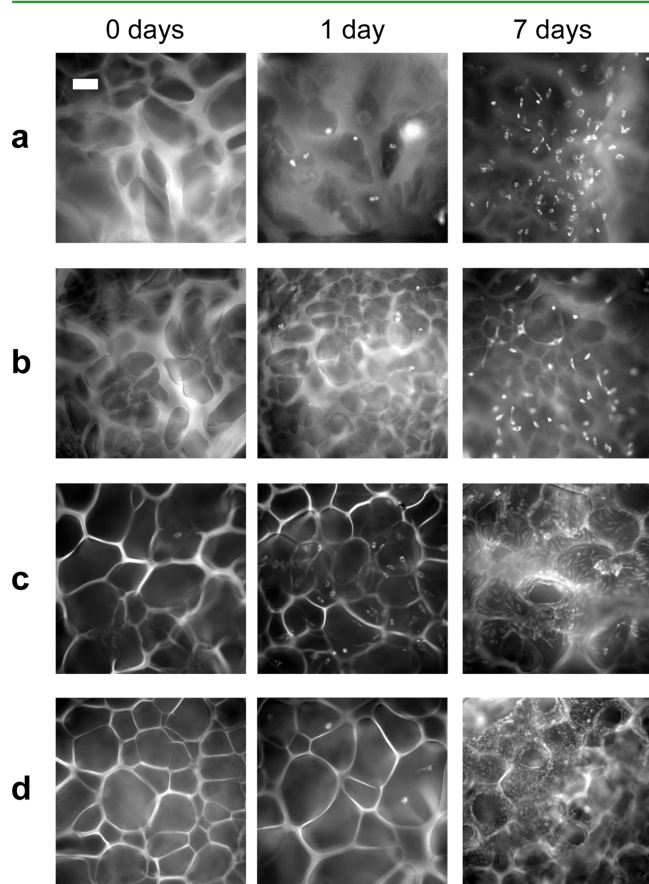

Figure 1. Fibroblast cell growth on scaffolds 1−4 assigned with a−d. Images in the first column show scaffold morphology, while the images in the second and the third column show cell growth after 1 and 7 days of culture, respectively. Images were taken using confocal fluorescence microscopy with 10× magnification. Scaffold polymers were labeled with fluorescein isothiocyanate (FITC) during fabrication and cells with SPP158 membrane probe prior analysis to acquire good fluorescent resolution and contrast. Results presented here are complemented with cell viability assay results shown in Figure 2b. The scale bar in the upper right corner represents 100 μm.

pair of scaffolds 1 and 2 and a pair of scaffolds 3 and 4, the statistical analysis (Figure 2a) cannot confirm this result as a significant one ($P = 0.135$; all the data compared simultaneously). The major problem originates in the high deviation of the cell number throughout the images due to generally low number of adherent cells that were counted over the limited field of view of 0.6 mm². To resolve this issue, cell growth was additionally analyzed with Resazurin cell viability assay,[48] which reaches better statistical relevancy by measuring the number of cells across the whole sample (Figure 2b). Analysis was done in six parallels. By this test, significant difference in cell growth between individual scaffolds was acquired already after 1 day of cell culture, with $P < 0.005$ when comparing scaffold 3 with 1 and 2 and $P < 0.001$ comparing scaffold 4 with 1 and 2, while no significant difference was acquired between pairs of scaffolds (1 and 2) and (3 and 4). The Resazurin assay thus clearly revealed that cell growth differentiates already during the first day of culture. In addition, the ratios between scaffolds remained practically unchanged for the whole week with no notable change in P value between individual pairs. The total number of cells on scaffolds was estimated from the Resazurin calibration curve (Figure S6 in the Supporting Information). Although the CFM analysis cannot adequately support the Resazurin results due to high deviation, it can on the other side provide insight into the cell morphology, proliferation, and migration through the scaffold. For example, efficient cell spreading around scaffold pores with more layers was observed on scaffolds 3 and 4, while less spreading with weak contact between cells was observed on scaffolds 1 and 2 (Figure 1, third column).

To understand the measured difference in cell growth established already during the first day (Figure 2b), we thus focused on the characterization of cell adhesion, a complex process involving integrin−ligand recognition followed by the launch of specific signaling pathways and cascades generating focal adhesions and further cell spreading and shape.[4]

Classification of Cell Adhesion. To search for correlation between initial cell adhesion and cell growth, adhesion dynamics was studied by using advanced system of optical tweezers combined with confocal fluorescence microscopy detection. During the analysis different adhesion strength was observed through the measured cell displacement within OT manipulation as depicted in Scheme 1b. Accordingly, three scenarios were defined, connecting different trap position dependent profiles of cell displacement and OT force induced on the interface (Scheme 2):

(a) In the case of high adhesion, the initial adhesion was too strong to be broken by the OT force of 100 pN. In this scenario the amplitude of cell displacement corresponds to the inverse number of integrin−ligand bonds at the interface. Due to strong adhesion slight cell displacement was observed only when the highest force was exerted (illustrated with D_1), i.e. when the optical trap was positioned in the region with the highest refractive index gradient Δn,[25] which is in the close proximity to the cell membrane (first vertical dashed line). When passing this point of the highest OT force, the cell could not be detached from scaffold. Instead, cell was released from the trap (illustrated with D_2) and shifted back to the initial position, due to release of the force-induced stretching (second vertical dashed line). Maximum amplitude of cell displacement of 5 μm was estimated
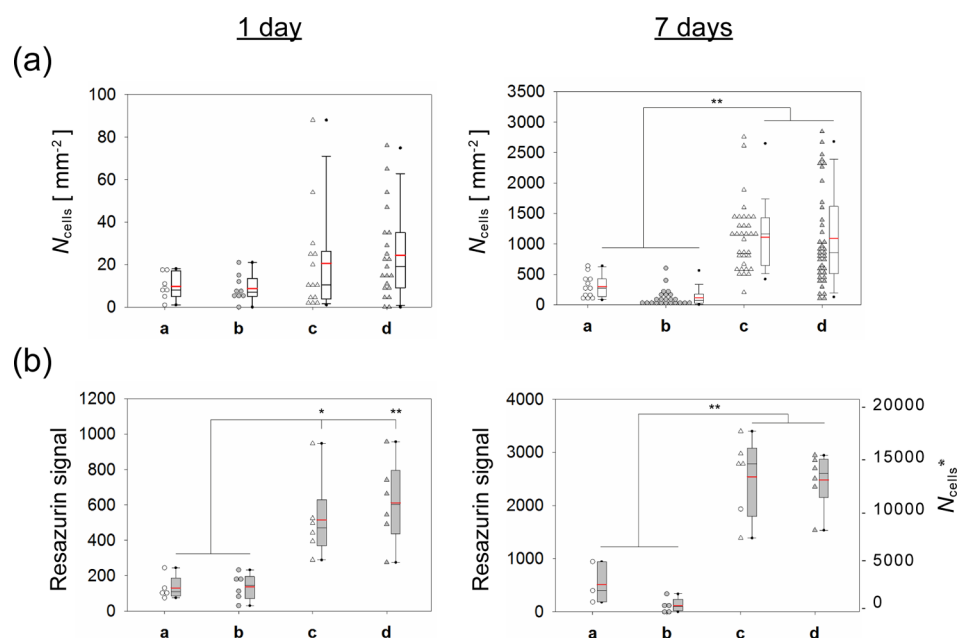
Figure 2. Cell growth of fibroblasts on scaffolds 1−4 assigned with a−d measured by a fluorescent detection of stained cells (a) and by Resazurin viability assay (b). Analysis was done after 1 and 7 days in culture. Measurements are represented with dot density plots with raw data on the left side of the bars. The boundary of the box closest to zero indicates the 25th percentile, lines within the box mark the median (black) and the mean (red), and the boundary of the box farthest from zero indicates the 75th percentile. Error bars above and below the box indicate the 90th and 10th percentiles. Data was correlated pairwise using statistical analysis: (*) $P < 0.005$; (**) $P < 0.001$. Optical detection was performed in three parallels each with 5−10 acquired images, and viability assay, in six parallels.

Scheme 2. Observed Scenarios of Cell Adhesion to the Scaffold Surface (a−c), Characterized with Optical Trap Position Induced Cell Displacement (Green) and OT Exerted Force (Blue)[a]
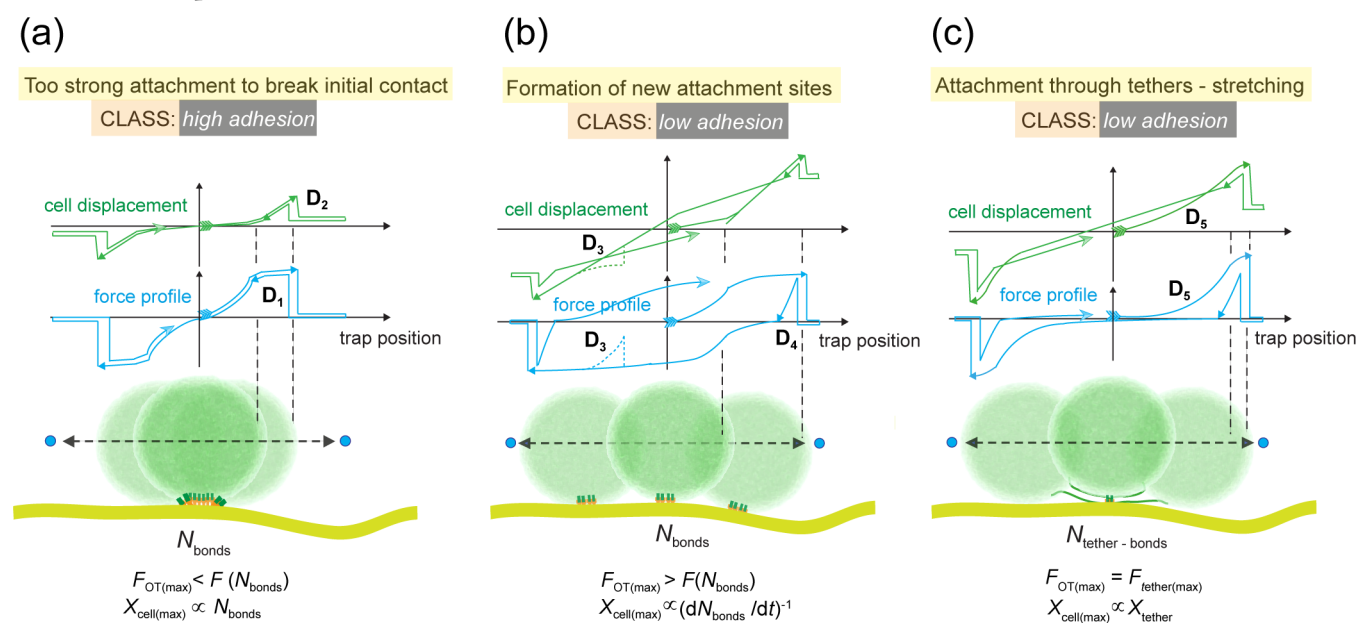
[a]The x axis shows the position of optical trap steadily moving from the center of a cell towards the cell membrane. In all cases, cell adhesion is strong enough to withstand the force of OT. However, different cell displacement points to different adhesion strength and mechanism: (a) small cell displacement is observed due to too strong adhesion to break initial attachment site; (b) high cell displacement is observed due to the breakage of initial attachment sites, where new ones are formed before cell detachment leading to rolling of the cell along the scaffold surface; (c) high cell displacement is observed due to formation a fluid tethers, through which adhesion is formed. They could be seen optically or recognized by OT induced cell displacement profile. The profiles have specific characteristics, which is denoted with characteristics $D_1 - D_5$: (D_1) slight cell displacement is observed when the highest force exerted with its profile unchanged by the direction of OT manipulation due to the type of adhesion; (D_2) cell displacement back into equilibrium position after the release of the stretched cell from a trap; (D_3) rapid increase in cell displacement and decrease in force induced on the interface due to bond detachment (optional); (D_4) bond stretching; (D_5) tether formation and tether growth.

for this adhesion type assuming geometrical and topological aspects of the cell surface with multidomain binding structures extending out of the lipid bilayer for 50 nm[46] accompanied by the surface microvilli of the size up to 500 nm,[49] and considering additional bond and cell stretching due to OT force.[50] Such an adhesion is presented in the movie clips am5b00235_si_003.avi and am5b00235_si_004.avi.

(b) In the case of low adhesion the amplitude of cell displacement was higher than 5 μm, meaning that OT force of 100 pN was strong enough to break the initial contact. However, new attachment sites were formed before cell detachment. In this scenario the amplitude of cell displacement corresponds to the inverse rate of bond formation while rolling the cell along the scaffold surface. By such a dynamic binding analogous to the rolling attachment mechanism of leucocytes to endothelium in a shear flow,[51−53] force can induce an increase in bond rupture during manipulation. The latter can be detected through the rapid increase in cell displacement caused by bond release which changes also the force profile (illustrated with D_3). Otherwise, the force profile is similar to the first scenario with high adhesion, as long as the trap is positioned within the cell where it experiences bond stretching (illustrated with D_4). Such an adhesion is presented in the movie clip am5b00235_si_005.avi in the Supporting Information, where rolling of the cell is observed accompanied by the breakage of the initial attachment sites, followed by formation of new ones. Note that the cell cannot move back to the initial position after the force is released.

(c) In another case of low adhesion cell binding is realized through the membrane tethers where cell displacement ranges from 5 to 20 μm. The amplitude corresponded more to the size of the extracted tether and not so much to the number of bonds formed through the tether or membrane−cytoskeleton tension, which was therefore approximated as being constant. Tethers were recognized through the cell displacement at small exerted force which is characteristic for lateral translocation/flow of lipids. In this roughly linear regime, force induced tether formation and stretching can be well described with spring constant,[54] where the force profile was of a similar shape as the cell displacement profile (illustrated with D_5). Note that the force induces flow of the lipids from the cell membrane reducing the cell internal volume and thus creating an increased pressure inside the cell. After the force is released, the internal pressure tends to increase the volume again by retracting the lipids from a tether back into the normal membrane state. This results in a backward motion of a cell toward the initial position (before force was applied). Binding through tethers with the visualized tether stretching and attachment point can be seen in the movie clip am5b00235_si_006.avi in the Supporting Information.

Each individual cell adhesion was classified with respect to the described cell attachment scenarios, which is presented in Table 2. The adhesion strength (1−4) was defined according to the measured amplitude of cell displacement. For cell displacement of less than 5 μm, cell adhesion type was identified as type (a) with adhesion strength 3−4. The number of bonds was roughly estimated according to the known

Table 2. Classification of Cell Adhesion According to the Amplitude of Cell Displacement

adhesion type	adhesion strength [0−4]	cell displacement [μm]	number of bonds[a] (N_{bonds})		
Scheme 2a	**4**−high	<1	>10		
	3−high	1−5	a few to 10		

adhesion type	adhesion strength [0−4]	cell displacement [μm]	binding rate (N_{bonds}/s)	OR	tether size
Scheme 2b OR c	**2**−low	5−15	>1		a few microns
	1−low	>15	$\cong$1		10 μm and more
	0.5	slow detachment	<1		/
	0	instant detachment	$\cong$0		/

[a]Number of bonds was estimated according to the experimental data of force per bond.[19,20,40,54]

experimental data of force per single integrin mediated bond with specific ECM amino acid sequence which was shown ∼50 pN after the interaction with collagen matrix,[18] ∼40 pN after interaction with RGDfK peptide,[20] and ∼20 pN after the interaction with fibronectin.[19] For cell displacement of more than 5 μm, cell adhesion type was identified with low strength (1−2) and as type b or c dependent on the characteristic force and cell displacement profile. Accordingly, binding rate (N_{bonds}/s) or tether size was roughly estimated. In case of nonadherent cells or cells detachable by the force of OT, the adhesion strength was identified with 0 or 0.5, respectively.

Seconds Scale Adhesion Dynamics Correlates with Cell Growth. As described, each cell adhesion experiment was characterized with the strength 0−4 and the corresponding time of contact which was represented with 2D Gauss probability profile:

$$f(t, \text{Adh}) = \exp\left(-\left(\frac{(t - t_0)^2}{2\sigma_t^2} + \frac{(\text{Adh} - \text{Adh}_{avg})^2}{2\sigma_{\text{Adh}}^2}\right)\right)$$

with the variances σ defined by corresponding measurement errors. By summation of all data points, contact time dependent distribution of adhesion strength was obtained as represented with contour plot (Figure 3). Final probability distributions were normalized to the number of data points.

The results of cell adhesion analysis are presented in Figure 4, where the measurements were done both in serum supplemented growth media DMEM and in PBS to check for the potential influence of serum proteins. Comparison between scaffolds 1−4 (a−d) was studied through the difference in distributions, taking into account adherent and nonadherent cells separately or all data points (adherent and nonadherent cells together). Adhesion strength was measured comprising only adherent cells, whereas determination of overall adhesion comprising all the data (Figure 4, third and fourth column). Cell adhesion was found to be significantly different between scaffold 2 and scaffold 3 with the P value of 0.01 and even more significantly different between the scaffolds 2 and 4 with P value of 0.001, both measured in growth media. In PBS, the significance is even more pronounced (lower P values for the correlation in both cases). Scaffold 1 was not identified as
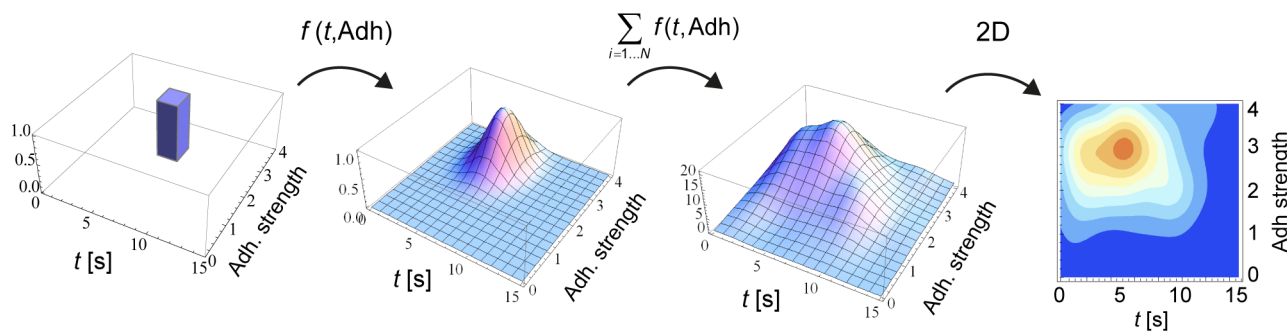
Figure 3. Construction of the contact time dependent adhesion strength probability distribution. Each analyzed cell adhesion was represented by a 2D Gauss function with the variances corresponding to the measurement errors ($\sigma_t = 1$ s and $\sigma_{Adh} = 0.5$). After summation of all data points, the distribution was represented with color-coded contour plots.
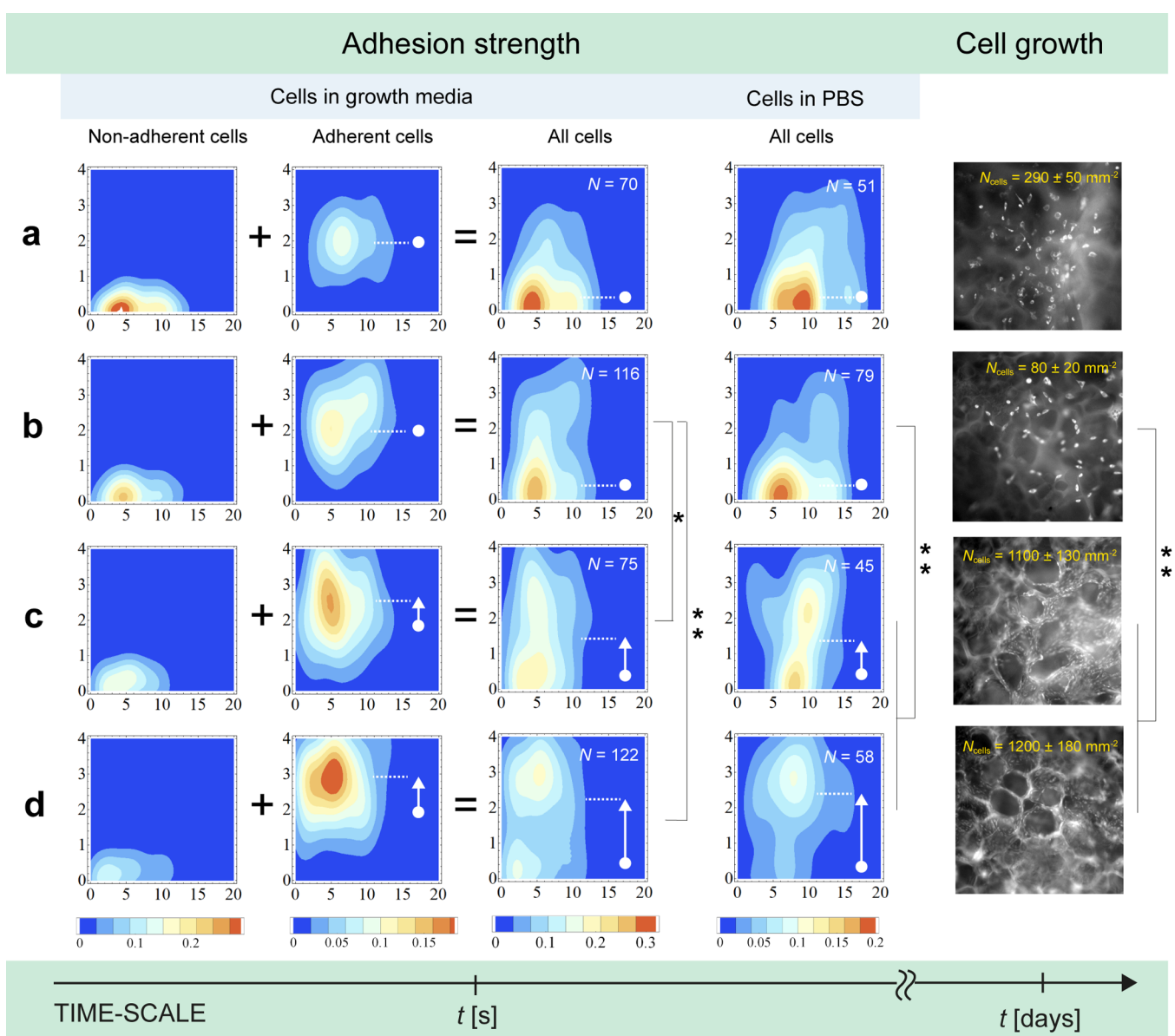

Figure 4. Distributions of cell adhesion on the surfaces of scaffolds 1−4 (a−d) measured in different media (first four columns) and the comparison with cell growth (fifth column). Adhesions strength was characterized with 0−4 (y-axis) after the contact time 0−20 s (x-axis). Distributions represented with contour plots were normalized to the number of analyzed cell adhesion events, with their number shown in the upper right corners. Besides, the increase of the average adhesion strength from the one on scaffolds with the lowest adhesion is depicted with white arrows. Raw data of cell adhesion events shown in Figures S7 and S8 in the Supporting Information was correlated pairwise using statistical analysis with (*) $P = 0.01$ and (**) $P = 0.001$.
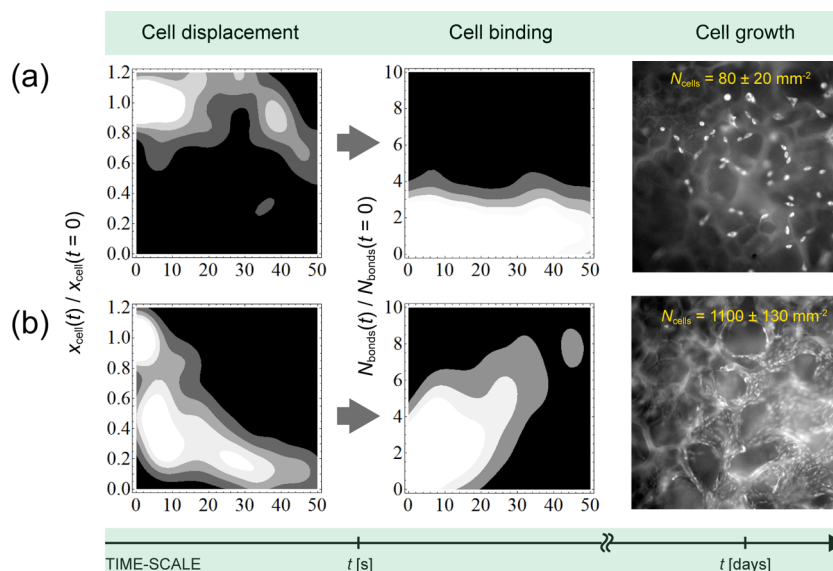
Figure 5. Dynamics of cell displacement normalized to the initial value at time $t = 0$ (first column) and bond formation rate (second column) on the surfaces of scaffolds 2 (a) and 3 (b). The corresponding cell growth is depicted in the third column. A higher density of data points is seen as brighter regions. The analysis on scaffolds 2 and 3 was obtained from 7 and 14 cell adhesion kinetics analysis, respectively.

significantly different from scaffold 2. The probability of the cell attachment might therefore play an important role in overall adhesion characterization. Being correlated with cell growth, the adhesion strength might therefore serve as an indicator to predict the initial cell growth.

By focusing back on the results of adhesion distribution analysis, a remarkable increase of probability of adhesion from scaffold 1 to 4 can be seen throughout the contour plots presented in first two columns. In addition, cells adhere to scaffold 1 to 4 with nearly increasing strength. This can be seen in the shift of the average value of adhesion distribution, i.e. in the shift of distribution maximum toward higher strengths (from 2 to 3). An increase of adhesion strength is indicated by the arrows with respect to the poor average adhesion strength on scaffolds 1 and 2, where the majority of cells did not establish strong attachment sites yet in the measured time window of a few to 10 s. Note that these few bonds are already strong enough not to be detached with the force induced by OT. Potentially, binding was to some extent governed through membrane tethers. However, scaffold 2 was identified with slightly wider distribution indicating more probable strong adhesion. On the other hand, the average adhesion strength on scaffolds 3 and 4 indicates that the majority of cells were able to establish strong attachment sites during this short time of contact, with more than just a few bonds (Table 2). The deficiency of serum proteins in PBS did not significantly modify cell adhesion as confirmed by statistical analysis (a slight time delay of adhesion when measuring in PBS cannot be confirmed as significant due to too low statistics in the acquired time range). This indicates that serum proteins do not impact the initial contact time and strength during the first few to ten seconds of adhesion, which is shown to be crucial for establishing first strong contacts. This finding is in accordance with some previous studies, where no significant effect of the presence of serum proteins was observed on cell growth on different polymer materials.[55] The latter can be explained either by the weak protein adsorption onto the highly hydrophilic surface of the scaffolds used in our study or by the barely changed scaffold surface by serum protein adsorption.[56]

To summarize, cell adhesion analysis in the first seconds showed good correlation with cell growth during the first week of culture. The fact that the majority of the adhesion events established binding forces stronger than 100 pN in about 5 s can additionally indicate how first-seconds time-scale binding events determine initial cell growth.

To understand the relationship between adhesion dynamics and cell growth more thoroughly, additional analysis of dynamic manipulation with OT was implemented. Beside the measurements of adhesion strength after particular time of the contact through which we estimated the number of bonds (Table 2), real-time dynamics of bonds formation was measured by dynamic OT manipulation of adherent cells as well (Scheme 1b). Cells were moved by periodical sequential optical trapping parallel to the scaffold surface, where the amplitude of cell displacement was measured in real-time. Time dependent cell displacement was then related to the time dependent number of bonds, and the last transformed into the rate of bond formation (Figure 5). By such manipulation, conditions analogous to the ones in vivo were mimicked, where cells in a shear flow adhere dynamically employing their rolling mechanism on adhesive surfaces.[51,52,57] Adhesion dynamics is thus not dependent just on the rate of receptor–ligand binding (k_{on}), their concentrations and their diffusion in the contact area as in the previous case, where adhesion strength was measured after static contact, but also on the considerable detachment rate (k_{off}) induced by the external force.[46,47] In our case, this was induced by OT with the loading rate dependent on the attachment scenario (Scheme 2) and maximum force of 100 ± 10 pN with the trap positioned close to the cell membrane.

The time dependent cell displacement and bond number evolution was analyzed on scaffolds 2 and 3, characterized with significantly different cell growth (Figure 2), to check if such analysis can also support different cell growth on scaffolds. Distribution of adhesion dynamics was again obtained with Gaussian representation of data (Figure 3) with the variances defined by measurement errors ($\sigma_t = 3$ s, $\sigma_{Disp} = 0.1$ and $\sigma_{Bonds} = 1$). Amplitude of cell displacement was normalized to the

initial value which was 4.8 ± 3.0 μm for scaffold 2 and 3.7 ± 2.8 μm for scaffold 3, indicating that the majority of analyzed cells on scaffold 3 was characterized with strong adhesion not being able to break the initial contact, while approximately half of the analyzed cells on scaffold 2 were characterized with low adhesion with thus lower ability of bond formation. Indeed, cell displacement shows dramatic difference between scaffold 2 and 3. On the time scale of 10 s to 1 min, the adhesion strength (number of bonds) is approximately 5 times larger in the case of scaffold 3 than in the case of scaffold 2. Since the analyzed binding dynamics depicts competition between attachment and detachment rates, k_{on} and k_{off} respectively, one quickly notices that k_{on} prevails over k_{off} on more biocompatible scaffold 3 even though the external force is constantly induced, endeavoring to break bonds[47] or to drastically decrease lifetime of bonds.[46] On less biocompatible scaffold 2, k_{on} and k_{off} seem to be of similar value. To sum up, the OT analysis revealed that the cell adhesion forces stronger than 100 pN can build up in the first few seconds. The observed results could serve to identify which scaffolds are suitable for efficient initial cell growth, a few orders of magnitude slower process.

CONCLUSION

Scaffold dependent cell growth measured throughout the first week of culture can be efficiently identified with cell adhesion dynamics on a second time scale. Cell adhesion strength in the acquired time interval applied by optical tweezers manipulation techniques and confocal fluorescence microscopy detection analysis was found to correlate with cell growth, clearly indicating that the first seconds of the contact can markedly direct further cell response. Such an adhesion analysis on 3D scaffold surfaces, applied for the first time, can thus represent a novel approach in gathering the essential information on initial cell–scaffold surface dynamics and more importantly can predict scaffold biocompatibility.

ASSOCIATED CONTENT

ⓈSupporting Information

Chemical structures of membrane fluorescent probes, calibration curve of Resazurin viability assay, movie clips of cell–scaffold adhesion dynamics experiments. This material is available free of charge via the Internet at http://pubs.acs.org.

AUTHOR INFORMATION

Corresponding Author

*E-mail: janez.strancar@ijs.si. Tel.: +386 (01) 477 3226. Fax: +386 (01) 477 3191.

Author Contributions

The manuscript was written through contributions of all authors. All authors have given approval to the final version of the manuscript.

Notes

The authors declare no competing financial interest.

ACKNOWLEDGMENTS

REFERENCES

(1) Williams, D. F. On the Mechanisms of Biocompatibility. *Biomaterials* **2008**, *29*, 2941−2953.

(2) Fisher, M. B.; Mauck, R. L. Tissue Engineering and Regenerative Medicine: Recent Innovations and the Transition to Translation. *Tissue Eng., Part B* **2013**, *19*, 1−13.

(3) Lee, M. H.; Arcidiacono, J. A.; Bilek, A. M.; Wille, J. J.; Hamill, C. A.; Wonnacott, K. M.; Wells, M. A.; Oh, S. S. Considerations for Tissue-Engineered and Regenerative Medicine Product Development Prior to Clinical Trials in the United States. *Tissue Eng., Part B* **2010**, *16*, 41−54.

(4) Hynes, R. O. Integrins: Bidirectional, Allosteric Signaling Machines. *Cell* **2002**, *110*, 673−687.

(5) Schwarz, U. S.; Safran, S. S. Physics of Adherent Cells. *Rev. Mod. Phys.* **2013**, *85*, 1327−1381.

(6) Bausch, A. R.; Schwarz, U. S. Cellular Mechanosensing: Sharing the Force. *Nat. Mater.* **2013**, *12*, 948−949.

(7) Hoffman, B. D.; Grashoff, C.; Schwartz, M. A. Dynamic Molecular Processes Mediate Cellular Mechanotransduction. *Nature* **2011**, *475*, 316−323.

(8) O'Brien, F. J. Biomaterials & Scaffolds for Tissue Engineering. *Mater. Today* **2011**, *14*, 88−95.

(9) Jin, G. Z.; Kim, H. W. Nanocomposite Bioactive Polymeric Scaffold Promotes Adhesion, Proliferation and Osteogenesis of Rat Bone Marrow Stromal Cells. *Tissue Eng. Regener. Med.* **2014**, *11*, 284−290.

(10) Huang, W. C.; Liu, K. H.; Liu, T. C.; Liu, D. M.; Chen, S. Y. Synergistic Hierarchical Silicone-Modified Polysaccharide Hybrid as a Soft Scaffold to Control Cell Adhesion and Proliferation. *Acta Biomater.* **2014**, *10*, 3546−3556.

(11) Collart-Dutilleul, P. Y.; Secret, E.; Panayotov, I.; Deville de Périère, D.; Martín-Palma, R. J.; Torres-Costa, V.; Martin, M.; Gergely, C.; Durand, J. O.; Cunin, F.; Cuisinier, F. J. Adhesion and Proliferation of Human Mesenchymal Stem Cells from Dental Pulp on Porous Silicon Scaffolds. *ACS Appl. Mater. Interfaces* **2014**, *6*, 1719−1728.

(12) García, A. J.; Ducheyne, P.; Boettiger, D. Quantification of Cell Adhesion Using a Spinning Disc Device and Application to Surface-Reactive Materials. *Biomaterials* **1997**, *18*, 1091−1098.

(13) Sniadecki, N. J.; Chen, C. S. Microfabricated Silicone Elastomeric Post Arrays for Measuring Traction Forces of Adherent Cells. *Methods Cell Biol.* **2007**, *83*, 313−328.

(14) Nugiel, D. J.; Wood, D. J.; Sung, K. L. Quantification of Adhesiveness of Osteoblasts to Titanium Surfaces In Vitro by the Micropipette Aspiration Technique. *Tissue Eng.* **1996**, *2*, 127−140.

(15) Reyes, C. D.; García, A. J. A Centrifugation Cell Adhesion Assay for High-Throughput Screening of Biomaterial Surfaces. *J. Biomed. Mater. Res., Part A* **2003**, *67*, 328−333.

(16) Helenius, J.; Heisenberg, C. P.; Gaub, H. E.; Muller, D. J. Single-Cell Force Spectroscopy. *J. Cell Sci.* **2008**, *121*, 1785−1791.

(17) Zhang, H.; Liu, K. K. Optical Tweezers for Single Cells. *J. R. Soc., Interface* **2008**, *5*, 671−690.

(18) Taubenberger, A.; Cisneros, D. A.; Friedrichs, J.; Puech, P. H.; Muller, D. J.; Franz, C. M. Revealing Early Steps of $\alpha 2\beta 1$ Integrin-Mediated Adhesion to Collagen Type I by Using Single-Cell Force Spectroscopy. *Mol. Biol. Cell* **2007**, *18*, 1634−1644.

(19) Thoumine, O.; Kocian, P.; Kottelat, A.; Meister, J. J. Short-Term Binding of Fibroblasts to Fibronectin: Optical Tweezers Experiments and Probabilistic Analysis. *Eur. Biophys. J.* **2000**, *29*, 398−408.

(20) Wang, X.; Ha, T. Defining Single Molecular Forces Required to Activate Integrin and Notch Signaling. *Science* **2013**, *340*, 991−994.

(21) Zhang, Y.; Ge, C.; Zhu, C.; Salaita, K. DNA-Based Digital Tension Probes Reveal Integrin Forces During Early Cell Adhesion. *Nat. Commun.* **2014**, *5*, 1−10.

(22) Capitanio, M.; Pavone, F. S. Interrogating Biology with Force: Single Molecule High-Resolution Measurements with Optical Tweezers. *Biophys. J.* **2013**, *105*, 1293−1303.

(23) Difato, F.; Pinato, G.; Cojoc, D. Cell Signaling Experiments Driven by Optical Manipulation. *Int. J. Mol. Sci.* **2013**, *14*, 8963−8984.

(24) Bowman, R. W.; Padgett, M. J. Optical Trapping and Binding. *Rep. Prog. Phys.* **2013**, *76*, 026401.

(25) Ashkin, A. In *Optical Trapping and Manipulation of Neutral Particles Using Lasers*; Ashkin, A., Ed.; World Scientific Publishing Co. Pte. Ltd.: Singapore, 2006; pp 1−915.

(26) Richardson, A. C.; Reihani, N.; Oddershede, L. B. Combining Confocal Microscopy with Precise Force-Scope Optical Tweezers. *Proc. SPIE* **2006**, 632628.

(27) Comstock, M. J.; Ha, T.; Chemia, Y. R. Ultrahigh-Resolution Optical Trap with Single-Fluorophore Sensitivity. *Nat. Methods* **2011**, *8*, 335−340.

(28) Thoumine, O.; Bard, L.; Saint-Michel, E.; Dequidt, C.; Choquet, D. Optical Tweezers and Fluorescence Recovery After Photo-Bleaching to Measure Molecular Interactions at the Cell Surface. *Cell. Mol. Bioeng.* **2008**, *1*, 301−311.

(29) Andersson, M.; Madgavkar, A.; Stjerndahl, M.; Wu, Y.; Tan, W.; Duran, R.; Niehren, S.; Mustafa, K.; Arvidson, K.; Wennerberg, A. Using Optical Tweezers for Measuring the Interaction Forces Between Human Bone Cells and Implant Surfaces: System Design and Force Calibration. *Rev. Sci. Instrum.* **2007**, *78*, 074302.

(30) Gou, X.; Han, H. C.; Hu, S.; Leung, A. Y. H.; Sun, D. Applying Combined Optical Tweezers and Fluorescence Microscopy Technologies to Manipulate Cell Adhesions for Cell-to-Cell Interaction Study. *IEEE Trans. Biomed. Eng.* **2013**, *60*, 2308−2315.

(31) Hu, S.; Gou, X.; Han, H.; Leung, A. Y. H.; Sun, D. Manipulating Cell Adhesions with Optical Tweezers for Study of Cell-to-Cell Interactions. *J. Biomed. Nanotechnol.* **2013**, *9*, 281−285.

(32) Podlipec, R.; Gorgieva, S.; Jurašin, D.; Urbančič, I.; Kokol, V.; Štrancar, J. Molecular Mobility of Scaffolds' Biopolymers Influences Cell Growth. *ACS Appl. Mater. Interfaces* **2014**, *6*, 15980−15990.

(33) König, K. Laser Tweezers are Sources of Two-Photon Excitation. *Cell. Mol. Biol.* **1998**, *44*, 721−733.

(34) Plieva, F. M.; Kumar, A.; Galaev, I. Y.; Mattiasson, B. In *Advanced Biomaterials*; Basu, B., Katti, D. S., Kumar, A., Eds.; John Wiley & Sons, Inc.: New Jersey, 2010; Chapter 14, pp 499−531.

(35) Gornall, J. L.; Terentjev, E. M. Concentration-Temperature Superposition of Helix Folding Rates in Gelatin. *Phys. Rev. Lett.* **2007**, *99*, 028304.

(36) Arsov, Z.; Urbančič, I.; Garvas, M.; Biglino, D.; Ljubetič, A.; Koklič, T.; Strancar, J. Fluorescence Microspectroscopy as a Tool to Study Mechanism of Nanoparticles Delivery into Living Cancer Cells. *Biomed. Opt. Express* **2011**, *2*, 2083−2095.

(37) Liu, Y.; Cheng, D. K.; Sonek, G. J.; Berns, M. W.; Chapman, C. F.; Tromberg, B. J. Evidence for Localized Cell Heating Induced by Infrared Optical Tweezers. *Biophys. J.* **1995**, *68*, 2137−2144.

(38) Ayano, S.; Wakamoto, Y.; Yamashita, S.; Yasuda, K. Quantitative Measurement of Damage Caused by 1064-nm Wavelength Optical Trapping of Escherichia Coli Cells Using On-Chip Single Cell Cultivation System. *Biochem. Biophys. Res. Commun.* **2006**, *350*, 678−684.

(39) Urbančič, I. *Response of Biomembrane Domains to External Stimuli*, Ph.D. dissertation, University in Maribor, Maribor, 2013.

(40) Litvinov, R. I.; Shuman, H.; Bennett, J. S.; Weisel, J. W. Binding Strength and Activation State of Single Fibrinogen-Integrin Pairs on Living Cells. *Proc. Natl. Acad. Sci. U. S. A.* **2002**, *99*, 7426−7431.

(41) Castelain, M.; Rouxhet, P. G.; Pignon, F.; Magnin, A.; Piau, J. M. Single-Cell Adhesion Probed In-Situ using Optical Tweezers: A Case Study with Saccharomyces Cerevisiae. *J. Appl. Phys.* **2012**, *111*, 114701.

(42) Simmons, R. M.; Finer, J. T.; Chu, S.; Spudich, J. A. Quantitative Measurements of Force and Displacement using an Optical Trap. *Biophys. J.* **1996**, *70*, 1813−1822.

(43) Schwingel, M.; Bastmeyer, M. Force Mapping during the Formation and Maturation of Cell Adhesion Sites with Multiple Optical Tweezers. *PLoS One* **2013**, *8*, e54850.

(44) Svoboda, K.; Block, S. M. Biological Applications of Optical Forces. *Annu. Rev. Biophys. Biomol. Struct.* **1994**, *23*, 247−285.

(45) Wu, Y.; Sun, D.; Huang, W. Mechanical Force Characterization in Manipulating Live Cells with Optical Tweezers. *J. Biomech.* **2011**, *44*, 741−746.

(46) Evans, E. A.; Calderwood, D. A. Forces and Bond Dynamics in Cell Adhesion. *Science* **2007**, *316*, 1148−1153.

(47) Bell, G. I. Models for the Specific Adhesion of Cells to Cells. *Science* **1978**, *200*, 618−627.

(48) Page, B.; Page, M.; Noel, C. A New Fluorometric Assay for Cytotoxicity Measurements In-Vitro. *Int. J. Oncol.* **1993**, *3*, 473−476.

(49) Gorelik, J.; Shevchuk, A. I.; Frolenkov, G. I.; Diakonov, I. A.; Lab, M. J.; Kros, C. J.; Richardson, G. P.; Vodyanoy, I.; Edwards, C. R. W.; Klenerman, D.; Korchev, Y. E. Dynamic Assembly of Surface Structures in Living Cells. *Proc. Natl. Acad. Sci. U. S. A.* **2003**, *100*, 5819−5822.

(50) Guck, J.; Ananthakrishnan, R.; Mahmood, H.; Moon, T. J.; Cunningham, C. C.; Kas, J. The Optical Stretcher: a Novel Laser Tool to Micromanipulate Cells. *Biophys. J.* **2001**, *81*, 767−784.

(51) Alon, R.; Hammer, D. A.; Springer, T. A. Lifetime of the P-Selectin-Carbohydrate Bond and its Response to Tensile Force in Hydrodynamic Flow. *Nature* **1995**, *374*, 539−542.

(52) Dong, C.; Cao, J.; Struble, E. J.; Lipowsky, H. H. Mechanics of Leukocyte Deformation and Adhesion to Endothelium in Shear Flow. *Ann. Biomed. Eng.* **1999**, *27*, 298−312.

(53) Spillmann, C. M.; Lomakina, E.; Waugh, R. E. Neutrophil Adhesive Contact Dependence on Impingement Force. *Biophys. J.* **2004**, *87*, 4237−4245.

(54) Schmitz, J.; Benoit, M.; Gottschalk, K. E. The Viscoelasticity of Membrane Tethers and its Importance for Cell Adhesion. *Biophys. J.* **2008**, *95*, 1448−1459.

(55) Schakenraad, J. M.; Busscher, H. J.; Wildevuur, C. R. H.; Arends, J. The Influence of Substratum Surface Free Energy on Growth and Spreading of Human Fibroblasts in the Presence and Absence of Serum Proteins. *J. Biomed. Mater. Res.* **1986**, *20*, 773−784.

(56) Dubruel, P.; Unger, R.; Van Vlierberghe, S.; Cnudde, V.; Jacobs, P. J. S.; Schacht, E.; Kirkpatrick, C. J. Porous Gelatin Hydrogels: 2. In Vitro Cell Interaction Study. *Biomacromolecules* **2007**, *8*, 338−344.

(57) Dong, C.; Lei, X. X. Biomechanics of Cell Rolling: Shear Flow, Cell-Surface Adhesion, and Cell Deformability. *J. Biomech.* **2000**, *33*, 35−43.